



# Design and offline testing of a resonant stripline beam position monitor for the IRFEL project at NSRL

Xiao-Yu Liu<sup>1</sup> · Fang-Fang Wu<sup>1</sup> · Tian-Yu Zhou<sup>1</sup> · Ping Lu<sup>1</sup> · Bao-Gen Sun<sup>1</sup>

Received: 28 February 2020 / Revised: 18 May 2020 / Accepted: 19 May 2020 / Published online: 25 June 2020

© China Science Publishing & Media Ltd. (Science Press), Shanghai Institute of Applied Physics, the Chinese Academy of Sciences, Chinese Nuclear Society and Springer Nature Singapore Pte Ltd. 2020

**Abstract** A 476 MHz resonant stripline beam position monitor (BPM) is planned to be installed in an infrared free electron laser machine at National Synchrotron Radiation Laboratory. This type of BPM was developed based on a standard stripline BPM by moving the coupling feed-through closer to the short end downstream, which introduces a resonance and therefore a capability for higher resolution compared with broadband BPMs. The design and offline measurement results of the prototype are shown in this paper. The design goal is the optimization of the central frequencies and corresponding quality factors of the three intrinsic transverse electromagnetic modes to roughly 476 MHz and 30, respectively, the fulfillment of which is demonstrated by a transmission parameter test via a network analyzer. Induced voltage signal modeling and an estimation of the position resolution of the designed BPM are shown in detail. Furthermore, a calibration test of the prototype using the stretched wire method is presented, including a description of the test stand and the evaluation of position sensitivities.

**Keywords** Beam diagnostics · Sensitivity · Resonant stripline BPM · Stretched wire method

---

This work was supported by the National Natural Science Foundation of China (Nos. 11575181, 21327901, 11705203), the Anhui Provincial Natural Science Foundation (No. 1808085QA24) and the Fundamental Research Funds for Central Universities (No. WK2310000080).

---

✉ Bao-Gen Sun  
bgsun@ustc.edu.cn

<sup>1</sup> National Synchrotron Radiation Laboratory, University of Science and Technology of China, Hefei 230029, China

## 1 Introduction

Beam position monitors (BPMs) [1–3] are essential elements in any particle accelerator for probing transverse beam positions. A reliable and precise BPM system is a precondition for the safe operation of accelerators. Therefore, in the last decades, technologies relating to BPMs have been studied extensively and rapidly developed.

Today, the most frequently utilized BPM devices include button BPMs [4–6], stripline BPMs [7, 8], and cavity BPMs [9–11]. The button BPM has the simplest structure and the most compact size; however, the induced signals are low due to the small electrode area. The standard stripline BPM has a comparatively larger induced signal and accordingly better signal to noise level ratio compared with the button BPM; however, the achievable position resolution is restricted by its intrinsic broadband property. The cavity BPM exhibits the best performance with respect to position resolution, but the high working frequency requires complicated post-processing electronics systems [12, 13], which results in a higher cost.

A newer type of beam position monitor, a resonant stripline BPM, was proposed in 2005 for proton beam measurements with a small beam current [14]. This type of BPM was modified, by moving the output coupler closer to the downstream end compared with the standard stripline BPM, which is shorted downstream. This modification leads to a resonant circuit with reduced bandwidth and a higher quality factor compared with the broadband stripline BPM, and therefore, a stronger induced signal and better resolution can be expected. Meanwhile, this modification does not result in any significant changes to the basic mechanical structure of a stripline BPM. Furthermore, this type of BPM does not have more extensive requirements

on the corresponding electronics system, and therefore, the same system as in button and stripline types of BPMs can be used.

A compact infrared free electron laser project [15] was built in NSRL. It has a tunable electron bunch repetition rate within 476 MHz and its fractional frequencies. Its electron beam energy ranges from 15 to 60 MeV, the micro-bunch charge is 1 nC, the micro-bunch length (rms) ranges from 2 to 5 ps, and the macro-pulse length ranges from 5 to 10  $\mu$ s. The requirements in terms of the transverse beam position resolution for macro-pulses are better than 50  $\mu$ m.

Owing to limitations in installation space, ten compact button-type BPMs, with button electrode positions deviating by 30 degrees from the horizontal axis, were designed as main diagnostic devices [16]. The Libera Single Pass E (Libera SPE) modules with a central frequency of 476 MHz and a 3 dB bandwidth of 10 MHz were selected for post-processing [17].

A resonant stripline BPM was also designed with the main purpose of studying on this newer type of BPM, considering its capability to provide a larger induced signal and the compatibility with the electronics Libera SPE. The cross section of a resonant stripline BPM contains one grounded chamber and four stripline electrodes. Owing to the coupling between the stripline electrodes, there exist three basic types of fundamental TEM modes inside a stripline-type BPM:

- Monopole mode  $(v_1, v_2, v_3, v_4) = \frac{1}{2}(1, 1, 1, 1)$ ;
- Dipole mode  $(v_1, v_2, v_3, v_4) = \frac{1}{\sqrt{2}}(0, 1, 0, -1)$  or  $(v_1, v_2, v_3, v_4) = \frac{1}{\sqrt{2}}(1, 0, -1, 0)$ ;
- Quadrupole mode  $(v_1, v_2, v_3, v_4) = \frac{1}{2}(1, -1, 1, -1)$ .

where  $v_1$ – $v_4$  are the voltages of the electrodes, starting from the electrode in the positive  $x$  direction and continuing in clockwise order. The electromagnetic field patterns of each mode are shown in Fig. 1

According to the coupling properties of each resonance mode, the mode frequencies should satisfy  $f_{\text{mono}} < f_{\text{dipole}} < f_{\text{quad}}$ , if no further modifications are made [14, 18]. To manage the induced signal, two basic solutions were proposed: (1) choose a central frequency of the electronics between the monopole and dipole resonant frequencies and avoid the case of their phase difference being equal to 90-deg [14, 19]; (2) optimize all resonant frequencies to the central frequency of the electronics system by widening the electrodes in the open end—the feasibility of this approach was successfully proven in the

design for the PSI-XFEL test injector [20, 21]. In our case, considering the systematical bandwidth of 10 MHz and the requirement of low cost, the second approach was chosen. It is worth noting that the tuning pins in Citterio et al.'s design, which were installed at the open end, are not used here due to their complex mechanical structures [20, 21]. The design goals for the resonant frequencies and quality factors are roughly 476 MHz and 30, respectively.

In the following, the details of the design and optimization of a 476 MHz resonant stripline BPM will be presented in Sect. 2; in Sect. 3, induced voltage signal modeling in the time domain will be shown in detail; the evaluation of the position resolution will be discussed in Sect. 4; offline tests, including measurements of resonant frequencies and quality factors and a test of the sensitivity of the fabricated prototype, as well as a simple analysis of the differences between the simulation and measurements will be shown in Sect. 5; a basic summary of this paper will be indicated in Sect. 6.

## 2 Design and simulation

The cross section of a resonant stripline BPM is shown in Fig. 2.  $R$  is the inner radius of the stripline electrode; it should be the same as the beampipe radius of 17.5 mm.  $T$  is the thickness of the stripline,  $D$  is the radial distance between the stripline and the vacuum chamber, and  $\theta$  denotes the coverage angle of the stripline.

Each stripline electrode and the grounded chamber form a transmission line, whose characteristic impedance  $Z$  under different TEM modes can be calculated via the Multipin Waveguide Port in CST [22]. The impedance  $Z$  has the relation  $Z \propto D/(\theta \cdot T)$  with the varying parameters  $D$ ,  $\theta$ , and  $T$ .

The basic model of a resonant stripline BPM is shown in Fig. 3a). The feedthrough divides the transmission line with a total length of  $L$  into two parts (of length  $L_1$  and  $L_2$ ). When looking from the feedthrough port to both parts, an equivalent circuit, as shown in Fig. 3b), can be introduced. In this circuit, the capacitance  $C_1$  replaces the  $L_1$ -part at the open end, the inductance  $L_{\text{eff}}$  replaces the  $L_2$ -part at the short end,  $C_p$  represents the parasitic capacitance due to the longitudinal gap (denoted as  $\text{gap}_z$  below) between the stripline and the vacuum pipe, and  $Z_0$  is the characteristic impedance of the feedthrough (50  $\Omega$ ).

Accordingly, resonant frequency  $f_0$  and external quality factor  $Q_e$  follow Eq. (1):

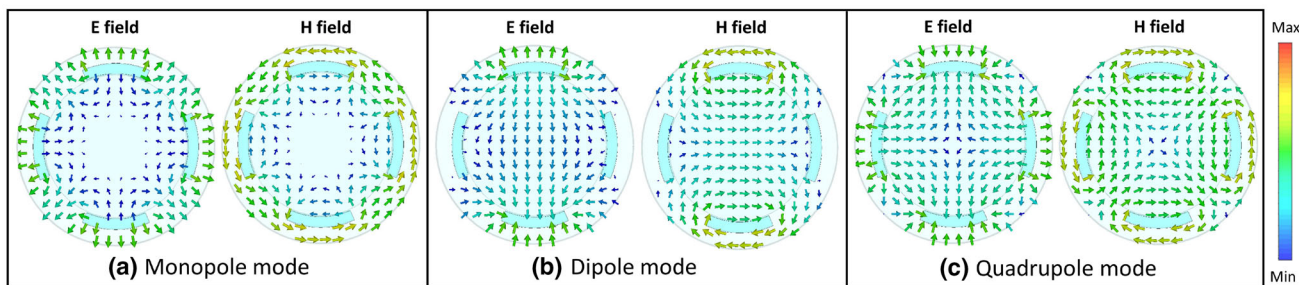


**Fig. 1** (Color figure online) The vector plots of the electromagnetic field patterns in the transverse  $x$ - $y$  plane corresponding to **a** monopole mode; **b** dipole mode; **c** quadrupole mode. Note that the field patterns of the dipole mode are only shown along the vertical direction  $y$

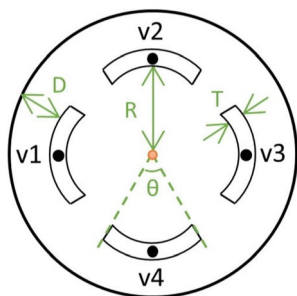


**Fig. 2** (Color figure online) Cross section of a resonant stripline BPM

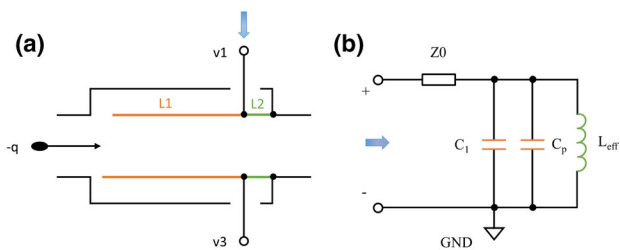


**Fig. 3** (Color figure online) Basic model of the resonant stripline BPM and its equivalent circuit from the point of view of the arrow, as marked

$$f_0 = \frac{1}{2\pi\sqrt{L_{eff} \cdot (C_1 + C_p)}},$$

$$Q_c = Z_0\sqrt{\frac{(C_1 + C_p)}{L_{eff}}}.$$
(1)

Based on transmission line theories [23] and the property of  $C_p$ , each component in Eq. (1) follows:

$$C_p \propto \frac{\theta \cdot T}{\text{gap}_z}$$

$$C_1 \propto \frac{L1}{Z}$$

$$L_{eff} \propto Z \cdot L2$$
(2)

As mentioned in Introduction, if no additional modifications of the structures are made, except for a movement of the feedthrough, the resonant frequencies of these three types of TEM modes should follow the relation:  $f_{mono} < f_{dipole} < f_{quad}$ . To optimize these three mode frequencies to be roughly equal, the stripline electrodes in the open end should be widened by an angle of  $\theta_{add}$ . By doing so, these three mode frequencies will decrease as a result of the equivalently higher  $\theta$ ; moreover, there is a further reduction in the modes, whose electrodes have different potentials (dipole and quadrupole modes); that is, the discrepancy between these three frequencies could be eliminated with a suitable  $\theta_{add}$ . A further optimization to the specific 476 MHz mainly relies on combined adjustments of the following parameters, shown in Table 1, which shows the basic options and the corresponding effects.

Based on these optimization rules, the designed prototype has mechanical dimensions as shown in Table 2,

Frequencies and quality factors are determined with the Microwave Studio of the CST package [22]; both the Eigenmode solver in the frequency domain and the Transient solver in the time domain are utilized for a cross-check. In the Eigenmode solver, all output couplers are assigned to a waveguide port to derive the external  $Q$ . The boundary conditions in the longitudinal direction are arbitrary, in case enough extra vacuum pipe is added in the simulation model, so that almost no field exists near the boundaries. In the Transient solver, the evaluation is based on the reflection parameter  $S_{11}$  at the feedthrough port for

**Table 1** Varied parameters and their corresponding effects

Option	Main effect
Fix $L$ , decrease $L2$	Higher $Q_c$
Increase $\theta_{add}$	Lower $f_{mono}$ $f_{dipole} - f_{mono}$ and $f_{quad} - f_{mono}$
Increase $\text{gap}_z$	Higher $f_0$
Increase $L$	Lower $f_0$

**Table 2** Main dimensions of the designed prototype

$T$	$D$	$\theta$	$L1$
2.5 mm	4 mm	45°	136.35 mm
$L2$	gap <sub>z</sub>	$\theta_{\text{add}}$	
15.15 mm	10 mm	3°	

specific combinations of excitation settings (i.e., Monopole mode corresponds to simultaneous excitation of the four ports in phase). At the resonant frequency  $f_0$ , group delay GD of  $S_{11}$  as a derivative of the phase change will reach the maximum  $\tau_0$  and the corresponding quality factor  $Q_0$  is approximately  $Q_0 = \pi f_0 \tau_0 / 2$ . Based on these two methods, the mode frequencies and  $Q$  factors of the final model are calculated as shown in Table 3 (the frequency resolution in the Transient is 0.2 MHz). The results indicate that the optimized mode frequencies could be considered to be equal.

### 3 Induced signal modeling

In the following, the induced voltage signal of the resonant stripline BPM is modeled based on the theory of cavity BPMs [9]. For a single bunch passing through a resonant BPM, the voltage seen by the charge along the trajectory  $l$  is

$$V = \left| \int_l E_z \cdot e^{ikz} dz \right| \tag{3}$$

where  $E_z$  is the electric field of the mode of interest. The exchange of energy between the bunch and the BPM can be characterized by the normalized shunt impedance:

$$\frac{R}{Q} = \frac{V^2}{\omega W} = \left[ \frac{R}{Q} \right]_{0,x_0^2} \tag{4}$$

where  $\omega$  is the mode resonance frequency,  $W$  is the energy stored in the BPM, and the shunt impedance  $[R/Q]_0$  corresponds to the beam trajectory with an offset of  $x_0$  from the electric center for the dipole mode. For the designed

**Table 3** Simulated mode frequencies and quality factors of the designed model via different solvers

Mode	Eigenmode solver		Transient solver	
	$f_0$ (MHz)	$Q_e \approx Q_1$	$f_0$ (MHz)	$Q_e \approx Q_1$
Monopole	476.46	30.82	475.30	31.44
Dipole	476.34	34.45	475.10	35.15
Quadrupole	476.49	36.71	475.50	37.62

BPM,  $[R/Q]$  of the monopole mode is  $25.91 \Omega$  and  $[R/Q]_0$  of the dipole mode for  $x_0 = 1 \text{ mm}$  is  $0.11 \Omega$ .

The energy left in an initially empty BPM after a Gaussian distributed bunch, which has a charge of  $q_b$  and a length of  $\sigma_t$ , passes through it can be calculated as

$$W = \frac{\omega q_b^2 R}{4 Q} e^{(-\omega^2 \sigma_t^2)} \tag{5}$$

Based on the definition of the external quality factor  $Q_e$  of the cavity as  $Q_e = \omega W / P_{\text{out}}$ , the power leaving the BPM can be expressed as

$$P_{\text{out}} = \frac{\omega^2 q_b^2 R}{4 Q_e Q} e^{(-\omega^2 \sigma_t^2)} \tag{6}$$

Then, the peak voltage out from the BPM along the transmission line with impedance  $Z$  is

$$V_{\text{out}} = \frac{\omega q_b}{\sqrt{2}} \sqrt{\frac{Z R}{Q_e Q}} e^{\left(-\frac{\omega^2 \sigma_t^2}{2}\right)} \tag{7}$$

As the energy stored in the BPM decays, the output voltage also decays exponentially with constant  $\tau = 2Q_l / \omega$ , where  $Q_l$  is the loaded quality factor. Therefore, the time behavior of the voltage signal is

$$V(t) = V_{\text{out}} e^{-\frac{t}{\tau}} \sin(\omega t) \tag{8}$$

Consequently, the voltage signals induced by the monopole and dipole modes of the resonant stripline BPM after a single bunch passing through can be represented by Eq. (9), where subscripts  $m$  and  $d$  correspond to the monopole and the dipole, respectively.

$$\begin{aligned} V_m(t) &= \frac{\omega_m q_b}{\sqrt{2}} \sqrt{\frac{Z}{Q_{m,e}} \left[ \frac{R}{Q} \right]_m} e^{\left(-\frac{\omega_m^2 \sigma_t^2}{2}\right)} e^{-\frac{t}{\tau_m}} \sin(\omega_m t) \\ V_d(t) &= \frac{\omega_d q_b}{\sqrt{2}} \sqrt{\frac{Z}{Q_{d,e}} \left[ \frac{R}{Q} \right]_{0,d}} \frac{x}{x_0} e^{\left(-\frac{\omega_d^2 \sigma_t^2}{2}\right)} e^{-\frac{t}{\tau_d}} \sin(\omega_d t) \end{aligned} \tag{9}$$

Based on these two equations, the voltage signals for a 2 ps single bunch carrying 1 nC charge passing through the BPM with an offset of 1 mm are shown in Fig. 4.

As the decay time is much longer than the bunch separation of 2.1 ns (476 MHz), subsequent bunches arrive before the signal induced by the first bunch has decayed. For a macro-pulse including  $N_{\text{bunch}}$  bunches with a repetition rate of  $f_{\text{RF}}$ , the signals should be expressed by the sum of the induced voltages of each bunch:

$$V_{(\text{macro}) m,d}(t) = \sum_{i=1}^{N_{\text{bunch}}} V_{m,d} \left( t - \frac{i-1}{f_{\text{RF}}} \right). \tag{10}$$

For a macro-pulse of length  $L_{\text{macro}}$  of 5  $\mu\text{s}$ , including bunches with a 1 nC charge, 2 ps length, and an offset of

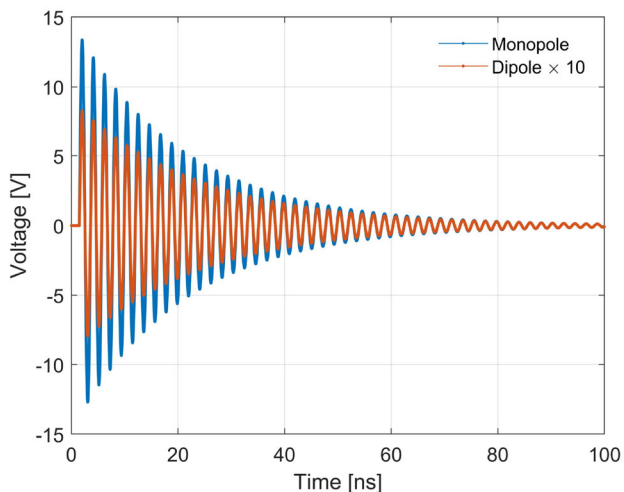


**Fig. 4** (Color figure online) Simulated voltage signals of the monopole and dipole modes of the resonant stripline BPM. A 2 ps single bunch with 1 nC charge and an offset of  $x_0 = 1$  mm is considered as the incident beam. Note that the dipole mode signal was scaled by a factor of 10 to improve visibility

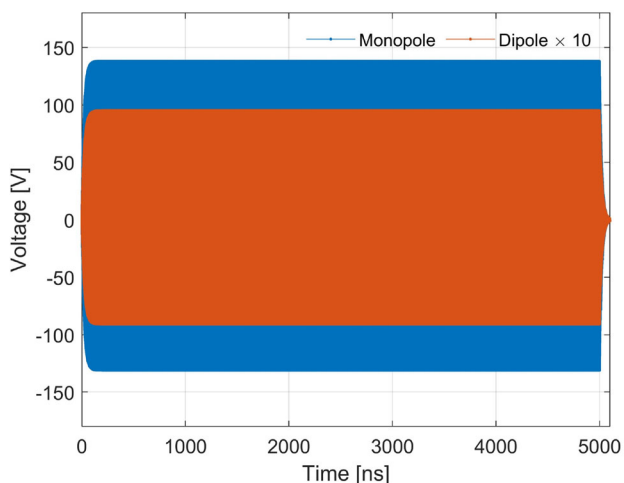


**Fig. 5** (Color figure online) Simulated voltage signals of the monopole and dipole modes of the resonant stripline BPM. A 5  $\mu$ s macro-pulse, including bunches with 1 nC charge, 2 ps length, and an offset of  $x_0 = 1$  mm is considered as the incident beam. Note that the dipole mode signal was scaled by a factor of 10 to improve visibility

$x_0 = 1$  mm, the corresponding mode signals are shown in Fig. 5.

The corresponding induced signals from the opposite electrodes of the BPM can be further deduced, as shown in Eq. 11, where the quadrupole mode is neglected.

$$\begin{aligned}
 v1(t) &= \frac{V_m(t)}{2} + \frac{V_d(t)}{\sqrt{2}} \\
 v3(t) &= \frac{V_m(t)}{2} - \frac{V_d(t)}{\sqrt{2}}.
 \end{aligned}
 \tag{11}$$

### 4 Estimation of position resolution

The position resolution of the BPM mainly depends on the signal-to-noise ratio and the position sensitivity. In the following section, an evaluation of the position sensitivity will be presented.

According to the analytical model described in the previous section, the voltage signal from BPM can be calculated in the time domain for any beam pattern. The corresponding signal in the frequency domain can be further derived via Fourier transform. As the Libera SPE is based on a 476 MHz bandpass filter, the signal level at this component is mainly concerned.

Therefore, the normalized position and a derived position sensitivity via the delta-over-sum method can be expressed as shown in Eq. 12, where  $v1(f)$  and  $v3(f)$  are the corresponding Fourier transforms of  $v1(t)$  and  $v3(t)$ :

$$U_{x,\Delta/\Sigma} = \frac{v1(f_0) - v3(f_0)}{v1(f_0) + v3(f_0)} \Big|_{f_0=476\text{MHz}},
 \tag{12}$$

$$S_{x,\Delta/\Sigma} = \frac{\partial U_{x,\Delta/\Sigma}}{\partial x} \Big|_{x=0}.$$

Based on this analytical model, the position sensitivity should follow the relation given in Eq. 13. For different beam patterns (i.e., different bunch length, bunch repetition rate, and pulse length), the derived sensitivities are all approximately  $0.098 \text{ mm}^{-1}$ .

$$S_{x,y} \propto \frac{\omega_{d(x,y)}}{\omega_m} \sqrt{\frac{[R/Q]_{0,d(x,y)}}{[R/Q]_m} \frac{Q_{m,e}}{Q_{d(x,y),e}}}
 \tag{13}$$

The Particle Studio of CST is used for analyzing the sensitivity, including the nonlinearity effect stemming from the quadrupole mode. As the simulation of macro-pulses can incur a heavy computational burden, the incident beam here was set to a 2 ps single bunch of 30 MeV energy and with a 1 nC charge. The electron bunch is swept along the horizontal direction,  $x$  within  $[-5, +5]$  mm, which indicates a sensitivity of roughly  $0.090 \text{ mm}^{-1}$  [18].

To further evaluate the position resolution, the RMS noise of Libera SPE with a varied input signal level was measured. The test followed the standard procedure presented in [17], with a continuous 476 MHz sine wave used as input. For the resonant stripline BPM with constant  $K_x = K_y = 11.11 \text{ mm}$  ( $K_{x,y} = 1/S_{x,y}$ ), the relation between RMS noise and input signal level is shown in Fig. 6.

The induced signal levels of the designed BPM, including a voltage range in the time domain  $V_{\text{range}}$  and power  $P_0$  of 476 MHz, for a centered beam with different bunch repetition rates are listed in Table 4. Note that the varied bunch lengths and macro-pulse lengths have no influence on the signal level.

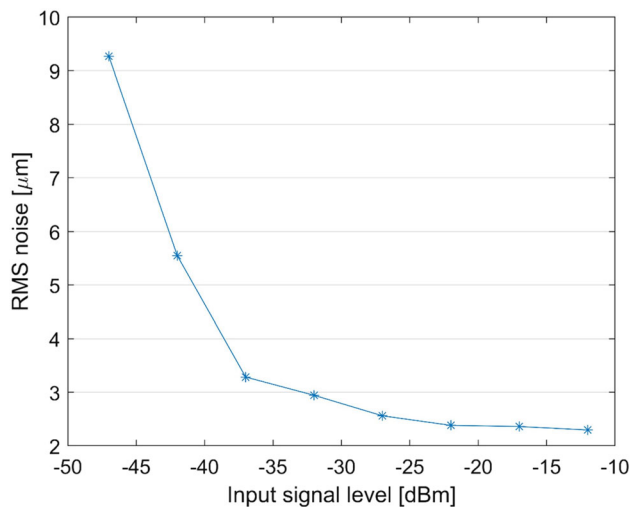


**Fig. 6** Measured RMS noise of Libera SPE versus input signal level

**Table 4** Simulated signal levels of the resonant stripline BPM for different bunch repetition rates

$f_{\text{RF}}$ (MHz)	$V_{\text{range}}$ (V)	$P_0$ (dBm)
476	– 65.5 to 69.0	46.4
238	– 34.4 to 36.2	40.3
119	– 19.0 to 20.0	34.3
59.5	– 11.4 to 12.0	28.4

As the acceptable power of Libera SPE is limited to roughly  $-12$  dBm, a combination of cable attenuation and extra variable attenuation will be used to fulfill this requirement. Further, considering a 5 dB margin for the beam offset,  $-17$  dBm is the final attainable signal level for any repetition rate listed in Table 4. Therefore, a resolution of roughly  $2.3 \mu\text{m}$  is expected for this BPM, that is, the requirement of a resolution better than  $50 \mu\text{m}$  can be well fulfilled [16].

## 5 Offline tests of prototype

Based on this design, one prototype, as shown in Fig. 7, was manufactured by Shenyang Huiyu Inc. The material of the vacuum chamber and the stripline electrodes is stainless steel 316LN. The feedthrough chosen is SMA type NL-108-564 [24] owing to its compatibility with this BPM. Contact between the inner conductor of the feedthrough and the stripline electrode is ensured by welding. The termination of the stripline downstream is effected by an extended circular piece, which is welded into the nearby flange.

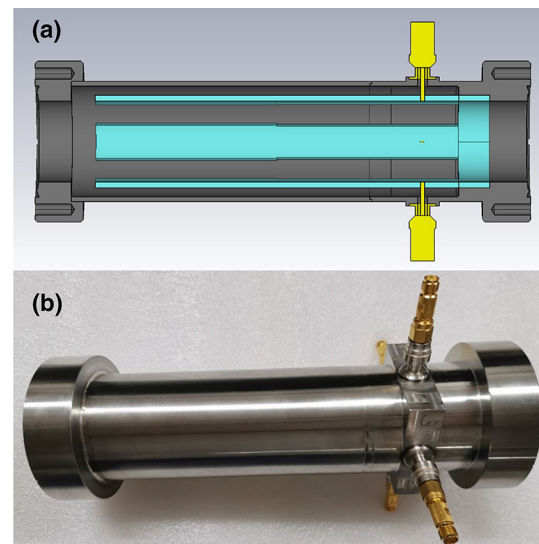


**Fig. 7** (Color figure online) Mechanical design of the BPM model and the fabricated prototype: **a** cross section of the mechanical design of the BPM model, from which the widening of the stripline electrodes near the open end is visible; **b** the corresponding BPM prototype after fabrication

The offline tests of this prototype mainly include two parts: (1) determination of resonant frequencies and  $Q$  factors based on the  $S$ -parameter measurements via Vector Network Analyzer (VNA); (2) evaluation of position sensitivity based on the stretched wire method [25].

The first test stand, where the group delay curves of the corresponding modes can be obtained, is shown in Fig. 8. At the beginning, it is necessary to calibrate the four ports of the VNA, including four SMA-to-SMA cables of 1 meter length, which are connected to the four feedthrough ports of the BPM on the other end. After that, a .s4p file data can be exported, which includes the full four-port scattering parameter matrix  $S_{ij}$  ( $i, j = 1, 2, 3, 4$ ) describing every possible combination of a response divided by a stimulus. The matrix is arranged in such a way that each column represents a particular stimulus condition, and each row represents a particular response condition. The standard four-port  $S$ -parameters matrix  $S_{\text{std}}$  is given as follows:

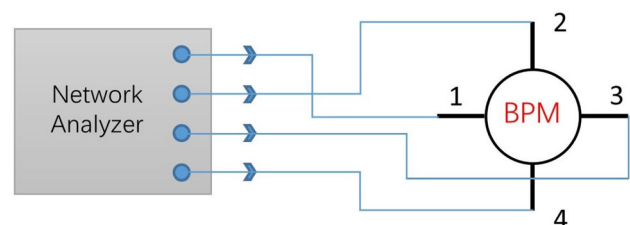


**Fig. 8** Test stand of mode resonance frequencies and quality factors of the resonant stripline BPM via the stretched wire method

$$S_{std} = \begin{bmatrix} S_{11} & S_{12} & S_{13} & S_{14} \\ S_{21} & S_{22} & S_{23} & S_{24} \\ S_{31} & S_{32} & S_{33} & S_{34} \\ S_{41} & S_{42} & S_{43} & S_{44} \end{bmatrix} \tag{14}$$

A mixed-mode  $S$ -matrix [26] as shown in Eq. 15 can be organized similarly to a single-ended  $S$ -matrix, in which each column (row) represents a different stimulus (response) condition. The mode information as well as the port information must be included in the mixed-mode  $S$ -matrix.

$$S_{mixed} = \begin{bmatrix} S_{d1d1} & S_{d1d2} & S_{d1c1} & S_{d1c2} \\ S_{d2d1} & S_{d2d2} & S_{d2c1} & S_{d2c2} \\ S_{c1d1} & S_{c1d2} & S_{c1c1} & S_{c1c2} \\ S_{c2d1} & S_{c2d2} & S_{c2c1} & S_{c2c2} \end{bmatrix} \tag{15}$$

$S_{didj}$  and  $S_{cicj}$ , ( $i, j = 1, 2$ ) are the differential-mode and common-mode  $S$  parameters, respectively. Among these,  $S_{d1d1}$  and  $S_{d2d2}$  correspond to the reflection parameters of the monopole and quadrupole modes, and  $S_{c1c1}$  and  $S_{c2c2}$  correspond to the reflection parameters of the two dipole modes.

The mixed-mode  $S$  parameters in Eq. 15 can be directly related to the standard four-port  $S$  parameters of Eq. 14. If ports 1 and 3, which are shown in Fig. 8, are paired as a single differential port, and ports 2 and 4 are paired as another differential port, the relationship between these two matrices can be described as follows:

$$S_{mixed} = MS_{std}M^{-1}, M = \frac{1}{\sqrt{2}} \begin{bmatrix} 1 & 0 & -1 & 0 \\ 0 & 1 & 0 & -1 \\ 1 & 0 & 1 & 0 \\ 0 & 1 & 0 & 1 \end{bmatrix} \tag{16}$$

According to calculations based on Eq. 16, the group delay curves derived by the reflection coefficients are shown in different colors in Fig. 9, as noted in the legend. It is worth mentioning that the group delay excludes the signal transmission time of the cables.

The measured mode frequencies and quality factors of the prototype are listed below, in Table 5.

The frequency resolution of the measurement is 0.25 MHz, in which case, the designed and measured mode frequencies are in good agreement, as all errors are within 1 MHz. This deviation might be due to machining errors in all designed dimensions, especially in the distance between the electrodes and the inner beam pipe near the open end, as there is no mechanical support of those parts and the stripline length is relatively long. Concerning the difference in quality factors, they might be caused by imperfections in the weld parts and inconsistencies between the

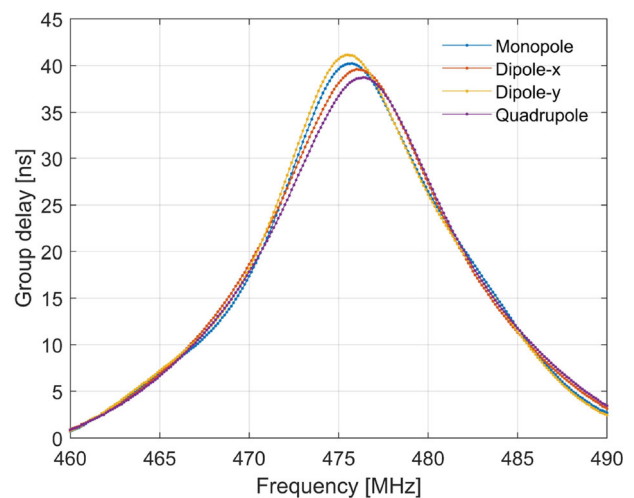


Fig. 9 (Color figure online) The group delay curves correspond to four resonant modes. Blue: monopole mode; red: dipole mode in  $x$  direction; yellow: dipole mode in  $y$  direction; purple: quadrupole

Table 5 Measured mode frequencies and quality factors of the BPM prototype

Mode	$f_0$ (MHz)	$Q_1$
Monopole	476.00	30.21
Dipole $x$	476.25	29.71
Dipole $y$	475.63	30.87
Quadrupole	476.25	29.06

material properties used in the simulation and in the fabrication.

The stretched wire method is a typical way to characterize the sensitivity of BPM. A typical test stand is shown in Fig. 10, where the BPM prototype is supported by a two-directional motor stage with a repeated positioning precision of a few microns. The 0.5 mm copper wire is fixed onto the two sides of the BPM and is stretched as tight as possible. The 476 MHz CW pulse fed into the wire will excite fields inside the BPM and induce corresponding voltage signals at the four feedthrough ports. We controlled the motor stage to make the location of wire be varied from  $[-5, -5]$  to  $[+5, +5]$  mm with respect to the electric center of BPM. The step sizes of the movement in both directions are 0.5 mm. The signals coupled out from the four ports are connected to the Libera SPE for further analysis. Based on measurements, the derived sensitivity in the horizontal direction  $S_x$  is approximately  $0.094 \text{ mm}^{-1}$  and the sensitivity in the vertical direction  $S_y$  is approximately  $0.088 \text{ mm}^{-1}$ , as shown in Fig. 11

The measured position sensitivities could generally be regarded as close to the theoretical value, although there is a difference between the vertical sensitivity  $S_y$  and the horizontal one  $S_x$ . According to Eq. 13 and the results shown in Table 5, the discrepancy between  $S_x$  and  $S_y$  is

**Fig. 10** (Color figure online) Test stand for position sensitivity of the resonant stripline BPM via the stretched wire method

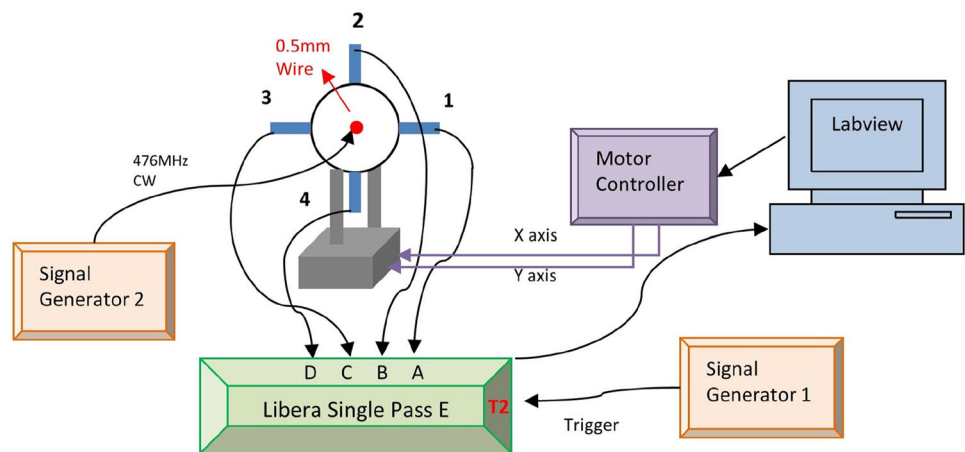
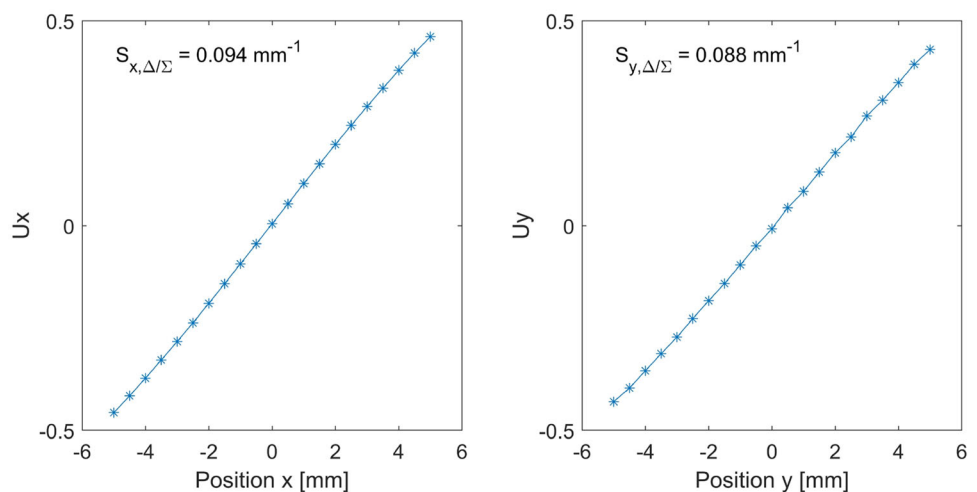


**Fig. 11** Measured position sensitivities of the resonant stripline BPM prototype via the stretched wire method



directly caused by the difference between the resonant frequencies and quality factors of these two dipole modes, as a result of fabrication errors.

## 6 Conclusion and outlook

In this paper, a design and offline tests of a 476 MHz resonant stripline BPM were introduced. Its main advantages are an increased voltage level out of the feedthrough due to a comparatively higher  $Q$  and its compatibility with the existing electronics of button-type BPMs. Both of these factors make this BPM a good choice for a more precise beam position measurement, as a position resolution of  $2.3\mu\text{m}$  can be expected for all beam patterns of our machine.

The mode frequencies and position sensitivities of the prototype were tested. All results show an acceptable deviation relative to the theoretical values, which indicates this BPM should work well with an electron beam.

This BPM could be also an option for noninterceptive emittance measurements, considering the existence of a triplet followed by a BPM in our facility, which was regarded as a stable implementation of a Miller's emittance measurement method via a four-electrode BPM [27, 28]. The corresponding work will be presented in the future, after machine commissioning is finished.

**Acknowledgements** The helpful discussions with M. Dehler, A. Citterio, M. Bopp, and A. Scherer are greatly appreciated. The assistance from Q. Wang and M. Qian in setting up the test platform is gratefully acknowledged; X. Y. Liu was supported by the China Scholarship Council for a 2-year study at PSI (Grant No. 201706340057), where the simulations were performed.

## References

1. R.E. Shafer, Beam position monitoring. AIP Conf. Proc. (1990). <https://doi.org/10.1063/1.39710>
2. P. Forck, P. Kowina, D. Liakin, *Beam position monitors*. CERN-2009-005 (2009)
3. C.X. Hong, C.M. Yang, P. Zhou et al., Study on X-ray beam stabilization of BL16B1 at SSRF. Nucl. Tech. **41**(12), 120101

- (2018). <https://doi.org/10.11889/j.0253-3219.2018.hjs.41.120101>. (in Chinese)
4. D. Lipka, B. Lorbeer, D. Noelle et al., Button BPM development for the European XFEL, *Paper Presented at the 10th European Workshop on Beam Diagnostics and Instrumentation for Particle Accelerators (DIPAC'11)* (Hamburg, Germany, May 2011)
  5. Z.C. Chen, Y.B. Leng, K.R. Ye et al., Beam position monitor design for a third generation light source. *Phys. Rev. ST Accel. Beams* **17**, 112801 (2014). <https://doi.org/10.1103/PhysRevSTAB.17.112801>
  6. Y. Zhang, J.X. Wu, X.C. Kang et al., Design of cold beam position monitor for CADS injector II proton LINAC, *Paper Presented at the Proceedings of the 2nd International Beam Instrumentation Conference (IBIC 2013)* (Oxford, UK, December 2013)
  7. T. Suwada, N. Kamikubota, H. Fukuma et al., Stripline-type beam-position-monitor system for single-bunch electron/positron beams. *Nucl. Instrum. Meth. A* **440**, 0168–9002 (2000). [https://doi.org/10.1016/S0168-9002\(99\)00960-2](https://doi.org/10.1016/S0168-9002(99)00960-2)
  8. F.F. Wu, Z.R. Zhou, B.G. Sun et al., Design and calculation of the stripline beam position monitor for HLS II storage ring, *Paper Presented at the 4th International Particle Accelerator Conference (IPAC'13)* (Shanghai, China, May 2013)
  9. S. Walston, S. Boogert, C. Chung et al., Performance of a high resolution cavity beam position monitor system. *Nucl. Instrum. Meth. A* (2007). <https://doi.org/10.1016/j.nima.2007.04.162>
  10. D. Lipka, Cavity BPM designs, related electronics and measured performances, *Paper Presented at the 9th European Workshop on Beam Diagnostics and Instrumentation for Particle Accelerators (DIPAC'09)* (Basel, Switzerland, May 2009)
  11. J.S. Zhou, J.S. Cao, Y.F. Sui et al., Design and simulation of cavity BPM for BEPCII. *Radiat. Detect. Technol. Methods* **3**, 49 (2019). <https://doi.org/10.1007/s41605-019-0125-z>
  12. L.W. Lai, Y.B. Leng, Y.B. Yan et al., Development and application of digital beam position measurement processor for FEL. *Nucl. Tech.* **41**(7), 070402 (2018). <https://doi.org/10.11889/j.0253-3219.2018.hjs.41.070402>. (in Chinese)
  13. Libera Cavity BPM. <https://www.i-tech.si/products/libera-cavitybpm/>
  14. M. Dehler, Resonant strip line BPM for ultra low current measurements, *Paper Presented at the 7th European Workshop on Beam Diagnostics and Instrumentation for Particle Accelerators (DIPAC'05)* (Lyon, France, June 2005)
  15. H.T. Li, Q.K. Jia, S.C. Zhang et al., Design of FELiChEM, the first infrared free-electron laser user facility in China. *Chin. Phys. C* **41**, 018102 (2017). <https://doi.org/10.1088/1674-1137/41/1/018102>
  16. X.Y. Liu, P. Lu, B.G. Sun et al., Design and simulation of button beam position monitor for IR-FEL, *Paper Presented at the 7th International Particle Accelerator Conference (IPAC'16)* (Busan, Korea, May 2016)
  17. Instrumentation Technologies, Libera Single Pass E specifications v1.02 (2014)
  18. X.Y. Liu, M. Bopp, M. Dehler et al., Design of resonant stripline BPM for an IR-FEL project at NSRL, *Paper Presented at the 10th International Particle Accelerator Conference (IPAC'19)* (Melbourne, Australia, May 2019)
  19. M. Dehler, G.J. Behrmann, M. Siemens et al., Stripline devices for FLASH and European XFEL, *Paper Presented at 2008 Beam Instrumentation Workshop (BIW'08)* (Lake Tahoe, CA, USA, May 2008)
  20. A. Citterio, M. Dehler, B. Keil et al., Design of a resonant stripline beam position pickup for the 250 MeV PSI XFEL test injector, *Paper Presented at the 9th European Workshop on Beam Diagnostics and Instrumentation for Particle Accelerators (DIPAC'09)* (Basel, Switzerland, May 2009)
  21. B. Keil, A. Citterio, M. Dehler et al., Commissioning of the low-charge resonant stripline BPM system for the SwissFEL test injector, *Paper Presented at the 32nd International Free Electron Laser Conference (FEL'10)* (Malmö, Sweden, Aug. 2010)
  22. Computer Simulation Technology. <https://www.cst.com/>
  23. D.M. Pozar, *Microwave Engineering*, 4th edn. (Wiley, London, 2011)
  24. Hitachi Haremachi Electronics Ltd. <https://www.hitachi.com/>
  25. D. Noelle, G.M. Priebe et al., BPMs with precise alignment for TTF2. *AIP Conf. Proc.* (2004). <https://doi.org/10.1063/1.39710>
  26. W. Fan, A. Lu, L.L. Wai, et al., Mixed-mode S-parameter characterization of differential structures, *Paper Presented at the 5th Electronics Packaging Technology Conference (EPTC 2003)*
  27. R.H. Miller, J.E. Clendenin, M.B. James, et al., *Nonintercepting emittance monitor*, United States: N. P. (1983) <https://doi.org/10.2172/5746569>
  28. S.J. Russell, Unstable matrix equations and their relationship to measuring the Emittance of an electron beam using beam position monitors. *Nucl. Instrum. Methods A* **430**, 498–506 (1999)